Exploring meteorological droughts' spatial patterns across Europe through complex network theory

Domenico Giaquinto[2], Warner Marzocchi[1,2], and Jürgen Kurths[2,3,4]

[1]University of Naples 'Federico II', Naples, Italy.
[2]Scuola Superiore Meridionale, Naples, Italy.
[3]Potsdam Institute for Climate Impact Research, Potsdam, Germany.
[4]Department of Physics, Humboldt University, Berlin, Germany.

Correspondence: Domenico Giaquinto (domenico.giaquinto@unina.it)

Abstract. In this paper we investigate the spatial patterns and features of meteorological droughts in Europe using concepts and methods derived from complex network theory. Using Event Synchronization analysis, we uncover robust meteorological drought continental networks based on the co-occurrence of these events at different locations within a season from 1981 to 2020 and compare the results for four accumulation periods of rainfall. Each continental network is then further examined
5   to unveil regional clusters which are characterized in terms of droughts' geographical propagation and source-sink systems. While introducing new methodologies in general climate networks reconstruction from raw data, our approach brings out key aspects concerning drought spatial dynamics, which could potentially support droughts' forecast.

1 Introduction

Droughts are among the most severe climate extremes, negatively affecting environments as well as societies and economies
10   (Taufik et al., 2017; Feng et al., 2021; Doughty et al., 2015; Walthall et al., 2013). As reported by the World Meteorological Organization (WMO, 2021), they were one of the most impactful natural hazard in terms of human losses during the period 1979 – 2019, accounting for 34% of disaster related deaths. To make matters worse, droughts are expected to grow and become more severe in the near future due to human related climate change (Spinoni et al., 2021). Additionally, although different drought types respond differently to increasing greenhouse gas concentrations and distinctions among geographic regions
15   should be made, there is high confidence that water stress is increasing globally according to the Sixth Assessment Report of the Intergovernmental Panel on Climate Change (IPCC) (Wehner et al., 2021).

Despite the high scientific interest and effort towards a better understanding of this crucial topic, there are still substantial discrepancies concerning the assessment of droughts' trends for specific regions. As for Europe, significant impacts have been extensively reported over the years, e.g. on ecosystems (Bastos et al., 2020), economy (Naumann et al., 2021), agriculture
20   (Beillouin et al., 2020). This climate phenomenon is closely monitored and studied both under present and future climate conditions (Spinoni et al., 2016; Marinho Ferreira Barbosa et al., 2021). When it comes to future scenarios, some studies claim that the entire continent will suffer under the increase of droughts' frequency and severity (Spinoni et al., 2018; Cook et al.,

2020). Others are more cautious in drawing such a conclusion, pointing out to the critical role of internal climate variability and associated uncertainties (Zhao and Dai, 2017; Vicente-Serrano et al., 2021). There are multiple reasons for these incongruences.

25 First of all, droughts are characterized by ample spatial variability (Vicente-Serrano et al., 2021): sub-continental or sometimes even sub-national areas behaves discordantly than their neighbors and different studies place emphasis on different territories (Spinoni J and P, 2016; Vicente-Serrano et al., 2021; Spinoni et al., 2018; Böhnisch et al., 2021). In addition, we lack a unique and standardized definition of regions: each scientific team outlines the sub-continental area of interest discretionally, following political or economic boundaries, according to the obtained results, or using external classifications (Spinoni J and

30 P, 2016; Spinoni et al., 2018, 2015). Although being completely understanding procedures, this makes comparisons among studies difficult, if not unfeasible.

On top of that, there is not a unique definition of drought. Depending on causes and impacts, droughts are classified into different types, i.e. meteorological, agricultural, hydrological and economic (Wilhite and Glantz, 1985; Seneviratne et al., 2012). These typologies are characterized by an increasing level of complexity, with impacts ranging from atmosphere to

35 land, ecosystems and even social and economic systems: an absolute definition could result in a misleading oversimplification (Lloyd-Hughes, 2014). Numerous indices have been proposed to classify, monitor and assess this complex climate event (Wei et al., 2021). Some are defined in terms of anomalies of a single variable, while, for the most complicated cases, multiple atmospheric variables are taken into account (Marinho Ferreira Barbosa et al., 2021). Each of them has its strengths and limitation (Mishra and Singh, 2010; Zargar et al., 2011; Wei et al., 2021; Mukherjee et al., 2018) behaving differently when

40 it comes to projections of future climate scenarios (Böhnisch et al., 2021; Vicente-Serrano et al., 2021). Using a hydrological and water-use model, Naumann et al. (2021) conclude that hydrological droughts' damages in Europe could strongly increase with global warming and cause a regional imbalance in future impacts. On the other hand, Vicente-Serrano et al. (2021) show that trends of meteorological droughts over Western Europe are statistically non-significant from a long term perspective.

Finally, the reference period used to identify the anomalies of the drought variable of interest, being it precipitation, soil

45 humidity, streamflow etc., represents another important source of inhomogeneity between different studies (Spinoni et al., 2017). Just as an example, Vicente-Serrano et al. (2021) use the period 1871–2018 to compute the Standardized Precipitation Index (McKee et al., 1993), while Spinoni et al. (2018) choose 1981–2010 to compute the frequency of drought events.

In this study we focus on meteorological droughts, defined as a period with a precipitation deficit in relation to the long-term average condition for a given region. Being simply related to precipitations, meteorological droughts are the basis for every

50 other drought class. A lack of precipitation may be the first precursor of soil humidity's reduction (agricultural drought) as well as the cause of stream flow shortage (hydrological drought) (Bevacqua et al., 2021).

The approach we propose in this study is based on complex networks and it is designed to address some of the criticalities described before, while detecting unknown spatial features of European meteorological droughts. Complex networks have been applied for many different purpose, e.g. to study social dynamics, power grids, epidemics and many others. They are a powerful

55 tool in systems composed of many units, where the interactions' structure is closely linked to system's dynamics (Boccaletti et al., 2006). Over the last two decades, complex network theory has been successfully applied to climate science too, proving to be an efficient method both to deepen our general understanding of various complex climate processes and to predict the

occurrence of extremes (Boers et al., 2019; Tsonis et al., 2006; Ludescher et al., 2021). Complex networks have been applied to droughts too. Ciemer et al. (2020) developed a forecasting scheme to predict the occurrence of meteorological droughts in the Central Amazon basin. In their recent paper, Konapala et al. (2022) develop a method to assess droughts' propagation in North America.

Our main objective here is to uncover spatial features of meteorological droughts in Europe, highlighting mechanism and patterns which could potentially support drought's forecast in the future. Our study is based on climate complex networks and on the concept of Event Synchronization, a nonlinear statistical similarity method useful to determine the correlations among spatial locations in terms of event co-occurrences. Using these tools we are able to identify drought regions in Europe based on the process itself and not depending on any external classifications, bringing out key aspects concerning drought dynamics at a regional scale for different rainfall accumulation periods from 1981 to 2020, while introducing new methodologies in general climate networks reconstruction from raw data. The understanding and ability of describing droughts as a complex phenomenon is still in a preliminary stage, but climate complex networks prove to be a powerful tool to reveal hidden features of this climatic process.

The reminder of the paper is organized as follows: in Section 2 we describe the data and the methodology we adopted to construct the meteorological drought networks and in Section 3 we present the results. Further insights and details on the methods are shown in the Appendix.

2   Data and Methodology

We follow the procedure described in Ludescher et al. (2021) and Fan et al. (2021) to reconstruct our meteorological droughts' networks from data, using the Standardized Precipitation Index (SPI) (McKee et al., 1993; Edwards, 1997; Guttman, 1999). The SPI measures precipitation's anomalies at a given location, based on a comparison of observed total rainfall for a certain accumulation time interval of interest (denoted SPI-1, SPI-3, SPI-6, SPI-9 and SPI-12 months) with the long-term historic record for that period and specific area (EDO, 2020). SPI values are positive (negative) for greater (less) than the median precipitation. The SPI is provided by the European Drought Observatory (EDO, 2020), computed from the monthly precipitation data of the Global Precipitation Climatology Centre. We focus on the time interval 1981 – 2020 and analyze four different accumulation periods, namely the SPI-3, SPI-6, SPI-9 and SPI-12, building one continental network for each of these cases, assessing their similarities and differences. The SPI-1 month is not considered, since it may not be accurate for regions with high probability of zero accumulated rainfall during one month (EDO, 2020), which is the case of some areas of northern Africa included in our study.

Our spatial domain is defined based on the IPCC's sixth assessment report (Jian and Hao-Ming, 2021; Iturbide et al., 2020): the regions NEU, WCE and MED are taken as representation of Europe (Figure 1). Notice that meteorological droughts are defined on lands and thus sea is not considered.

The spatial domain is discretized with a resolution of $0.25° \times 0.25°$ (latitude x longitude). Each grid point is associated to four SPI series (one for each accumulation period) and will serve as node of the graph.
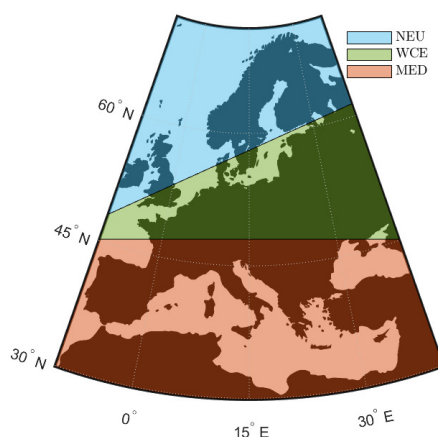
Figure 1. The spatial domain analyzed in this study using the IPCC regions NEU, WCE and MED (only lands are considered). Latitude from $30°$ to $72.6°$ and Longitude from $-10°$ to $40°$.

To identify meteorological droughts in the SPI time series we refer to McKee's work (McKee et al., 1993), where the author proposes a functional and quantitative definition of drought using the SPI as indicator: a meteorological drought is an event that occurs whenever the value of the SPI ≤ -1, whatever the accumulation period is. This definition and the related drought's classes (Table 1) are still accepted and wildly used (Spinoni J and P, 2016; WMO, 2021). The event sequences from the complete SPI time series are recovered by selecting those occurrences with SPI ≤ -1 and consecutive events are removed, keeping only the first of successive drought conditions (see Figure 2).

Table 1. Meteorological drought categories defined for values of the SPI from (McKee et al., 1993).

SPI values	Drought category
-1 to -1.49	moderate drought
-1.50 to -1.99	severe drought
$\leq$ -2	extreme drought

According to the event-like nature of this process, we use Event Synchronization (Quiroga et al., 2002; Malik et al., 2012) as statistical similarity measure to construct each of the four continental drought networks. Event synchronization is a powerful nonlinear method to assess the similarity of event series with not equal spacing between successive occurrences and thus it is especially appropriate for studying extreme events (Fan et al., 2021). The degree of synchronicity of two event series is measured based on the relative timings of events and it is obtained from the number of quasi-simultaneous occurrences. The detailed algorithm is described in Fan et al. (2021) and is shortly repeated in the Appendix for the convenience of the reader. The edges derived through Event Synchronization represent the synchronicity in drought's occurrences between the nodes of

the graph. In this preliminary stage, we are not concerned with the direction of synchronicity: two location are linked if they

105 display a co-evolution of meteorological drought events; therefore, the resulting four continental networks are undirected.
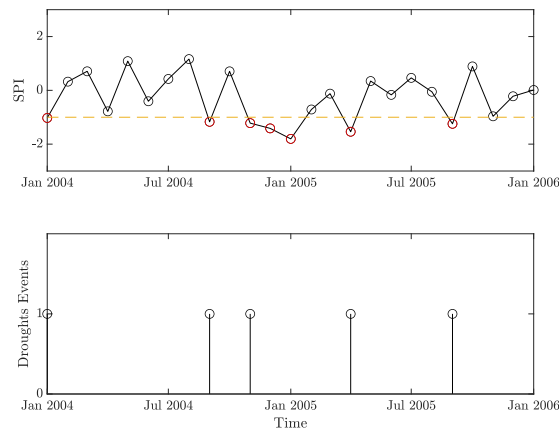
Figure 2. Construction of the Event Series. From the complete SPI Time Series (top panel) we select those realizations with SPI ≤ -1 to form the Droughts Event Series (bottom panel). Notice that consecutive events are removed, keeping only the first occurrence. This procedure is carried for every node of the space domain and for the entire time period 1981 - 2020.

The connections contained in the four continental networks have different strengths, i.e. value of synchronicity degree (see equation A4). Given the large extension and the high resolution of these graphs, it is not essential to carry the information of links' weights: instead, it is more convenient to select only the strongest edges and derive unweighted representations of each network (see equation A5), which will still preserve the main structures of the original graphs.

110 Extracting the connections with the highest statistical similarity from the complete weighted graph is a very common procedure in general functional network reconstruction from raw data (Zanin et al., 2012), and it is well known in climate networks science too (Ludescher et al., 2021; Gupta et al., 2021; Ciemer et al., 2020). In this particular field, the strongest links are considered to be the backbone structure of the climatic process under examination: indeed, when a climate correlation or synchronization network is built, it often resembles an all-to-all connected graph, giving no useful information about the main

115 underlying structure which remains hidden under the great number of links. Cutting-off the weakest edges is thus a fundamental step to get a clearer and meaningful representation of any climatic process (equation A5). Still, we lack so far a systematic and well accepted procedure to select this cut-off threshold θ in A5 for climate networks, and, moreover, to assess the robustness of the selected connections. As a result, scientists tend to choose it discretionally on a case by case basis (Kurths et al., 2019), generally optimizing the ratio between high correlation and sufficient number of events for comparison (Stolbova et al., 2014).

120 Here we propose a rigorous way to choose the lower bound of synchronicity below which a connection is discarded based on the Hamming distance (equation B1 and B2).

Instead of constructing one 1981-2020 drought network for each accumulation period, we divide the complete data-set into two sub-databases and build two independent sub-networks; we then choose the cut-off threshold which minimizes the

Hamming distance between these two sub-networks (Figure B1). With this procedure we not only identify the best cut-off
125 threshold, but we have the additional advantage of selecting the connections which are significant and robust in time because
they arise from independent sets of data: the network so reconstructed does indeed retain the long lasting backbone structure
of the process, discarding the majority of the spurious synchronizations caused by internal variability and noise. More details
about this method are given in the Appendix.

After having built the four unweighted and undirected European networks, we proceed in partitioning them into regional
130 clusters. This procedure is followed in Konapala et al. (2022) as well, where the authors use a distance weighted synchro-
nization to construct the graph. This filter strengthens the synchronicity among close locations, while penalizing any potential
connection between distant areas. Moreover, the distance weight introduced by Konapala et al. (2022) is a relative metric,
tuned on the extent of the studied domain. Even assuming that drought conditions' propagation is influenced by geographical
distance and therefore bounded to a certain level, this sensitivity should at least be fixed, not changing with the size of the
135 studied area. Whereas according to the majority of studies in climate networks long connections can not be ignored; on the
contrary, teleconnections play a crucial role in transferring climate information across the globe (Donges et al., 2009; Tsonis
et al., 2008, 2006; Boers et al., 2019, 2013; Stolbova et al., 2014). These considerations prompts us to identify regional clusters
from the Event Synchronization network without introducing any distance weight.

To find the regional clusters for each of the four networks, we use the Louvian algorithm (Blondel et al., 2008), a heuristic
140 method that is based on modularity optimization (Newman, 2006). The Louvian algorithm finds a local maximum of modular-
ity, which depends on the order the nodes are picked. Therefore, we apply it 10,000 times for each continental network, taking
the partition with the overall highest modularity. The found communities represent the regions in which a drought event is more
likely to propagate once started: intra-connections are maximized over inter-connections, meaning that the nodes grouped to-
gether are characterized by a high cooperativity in terms of synchronization in meteorological droughts' occurrences.

145 To analyze the synchronization's patterns of meteorological droughts, we build regional spatial networks for each commu-
nity. This time, unlike what was done before for the four continental networks, once the nodes of one specific community are
extrapolated, we use Event Synchronization to build weighted and directed graphs.

The comparison between the four continental networks and the features of the regional networks are described in the next
Section.

3 Results

150

The partitions of the four European drought networks resulting from 10,000 different realizations of the Louvian algorithm are
shown in Figure 3.

We notice important similarities and differences between the four networks. The most relevant features that arise are the
following: i) the regional clusters of the Scandinavian Peninsula are quite comparable, with the western part of Norway always
155 standing alone as one community, separated from Sweden, which forms another compact block, and Finland, often divided
into several parts alongside the Kola Peninsula; ii) the eastern part of the continent is split into latitudinal regions, well visible

(a) (b)

(c) (d)
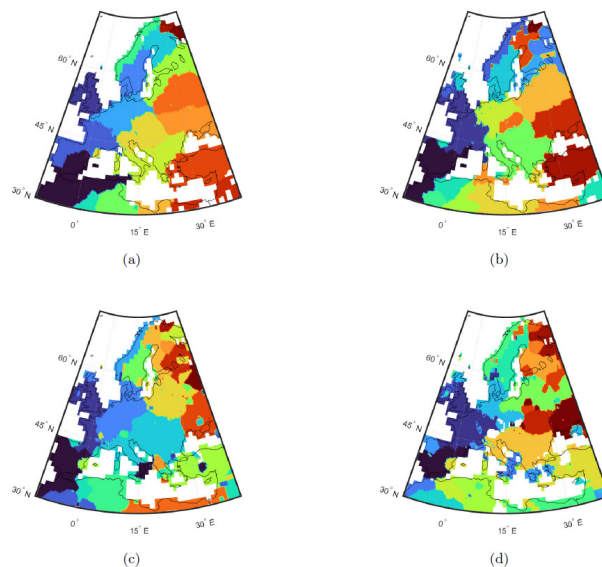
Figure 3. Communities detected with the Louvian algorithm from the SPI-3 Network (a), SPI-6 Network (b), SPI-9 Network (c) and SPI-12 Network (d). Each color represents a different community while white areas are either part of the sea or consist of nodes belonging to clusters with less than 100 nodes.

for the shortest accumulation periods while more and more fragmented in the 9 and 12 months cases; iii) Turkey often forms one cluster; iv) the Iberian peninsula is connected to North-west Africa, except for the SPI-12 network; v) the norther part of Italy is joined with the north of the Balkan Peninsula; vi) the increase of the fragmentation of the communities with the accumulation period does not translate into an increment of the communities' number (see Table 2), but to the disruption of the spatial continuity of the clusters from the shortest accumulation periods to the longest one.

We find that the latter characteristic is due to the presence of long links, more numerous the higher the accumulation period: we register 25565 long links in the SPI-12 Network, one order of magnitude more than the 2722 long links in the SPI-3 Network (see Figure 4 and Table 2). In Boers et al. (2019) the extreme precipitations' global climate network was characterized by two different weather systems, a regional power-law distributed one and a super-power-law-distributed global pattern. This latter system was detected from network's links longer than 2500 kilometers. In our analysis, these features seem to emerge again, even if we focus on negative precipitation's extremes and Europe is not big enough to contain a statistically adequate number of possible long connections ($\geq$ 2500 km). Nevertheless, if we look at Figure 4, we see a shift in the distribution of the number of links when this critical 2500 km length is passed. Moreover, the number of long links increases with the accumulation period, even when the total number of connections does not change sensibly among the four cases (see Table 2).

This exhibits the primary role of long connections in the context of climate networks. The presence of these long links is typically due to large scale atmospheric patterns which could act as common drivers of climate extremes of distant regions. This feature would not emerge if we used a distance weighted network's construction: in fact, we would have lost long con-
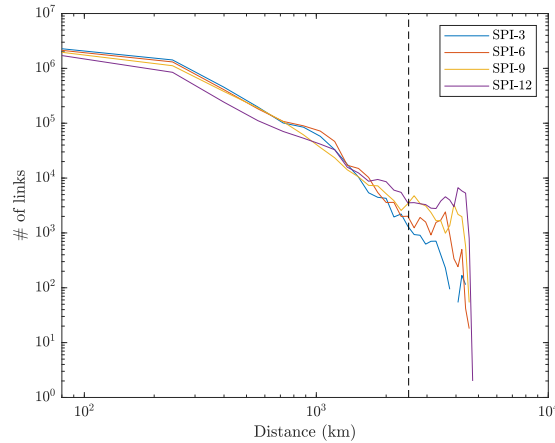
Figure 4. Distribution of the number of links with their traveled distance (great circle distance of the two nodes connected by the link) for each of the four Europe's meteorological drought networks (colored lines). Distance of 2500 km (dashed line.)

Table 2. Number of total and long links ($\geq$ 2500 km) in the four Europe's meteorological drought networks and number of found communities.

	Total Links	Long Links ($\geq$ 2500 km)	% of long links	Communities
SPI-3 Network	2340806	2722	0.12	19
SPI-6 Network	2210586	7074	0.32	19
SPI-9 Network	1979005	14599	0.74	19
SPI-12 Network	1615415	25565	1.58	21

nections, being left with four partitions very similar one to the other. We argue that short meteorological drought events (with

175   accumulation period up to 6 months) are driven by regional climate systems, while long ones (with accumulation period from 9 months onward) are due to large scale patterns that affects ample portion of the continent. Rossby wave trains could be a potential reasonable candidate in connecting distant area in longitudinal direction. Following studies could better clarify the climate precursors responsible for the appearance of these long connections for high accumulation periods.

     Once we identify the clusters of each of the four continental networks, we proceed in studying each regional community

180   separately, constructing weighted and directed graphs. The antisymmetrical score q_{ij} (Equation A4) which results from the application of Event Synchronization (see the Appendix) to the regional clusters can be used to derive the out-degree k_i^{out} (defined as the average of the weights of the outgoing links) and the in-degree k_i^{in} (defined as the average of the weights of the

incoming links) of each node i in its community c and, consequently, its overall degree centrality k_i:

$$k_i = k_i^{out} + k_i^{in} = \frac{1}{N_c - 1} \sum_{j \in \mathcal{N}_i} q_{ij} + \frac{1}{N_c - 1} \sum_{j \in \mathcal{N}_i} q_{ji} \tag{1}$$

185   where N_c is the total number of nodes belonging to community c and $\mathcal{N}_i$ are the neighbors of node i. The degree centrality k_i lies between -1 and 1. Here, a node i with $k_i < 0$ is defined as a sink, otherwise as a source. Each community of each of the four continental networks can be thus studied under this framework, identifying a source-sink system.

We show here some interesting source-sink systems found in each of the four continental networks.
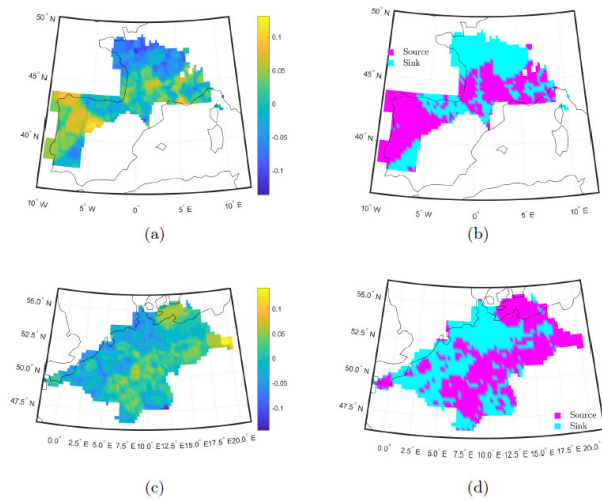
Figure 5. Two regional spatial networks from the SPI-3 Europe meteorological drought network. Degree centrality (a, c) and source-sink system (b, d).

In the SPI-3 network Portugal essentially acts as a source for its community (Figures 5a and 5b), suggesting that the lack of
190   humidity could move from the ocean towards the continent. A different situation is depicted in the central Europe community (Figures 5c and 5d), where the internal part of the region drives droughts' occurrences to the coasts. In the SPI-6 networks, it is interesting to notice the connection between northern Ireland and the Norwegian mountains (Figures 6a and 6b). As we already pointed out looking at Figure 3, the western part of Norway is always separated from the rest of the Scandinavian peninsula in every of the four accumulation periods networks, but in the specific case of the SPI-6 network, it seems that northern Ireland
195   has a certain synchronicity with this mountainous chain and in particular it uniformly acts as a sink. Another regional spatial network derived from the SPI-6 graph that we show here is the Turkey one. We mentioned that this region often consistently form one sole cluster, displaying a certain stability over the different accumulation periods cases. In the SPI-6 network the western and central regions of Turkey precede the East in the occurrence of meteorological droughts events (Figures 6c and 6d). For the SPI-9 network we show two communities which are somehow complementary to each other (Figure 7): the first one (Figures 7a and 7b) includes the majority of the Iberian peninsula with a small region of Turkey while in the second one
200
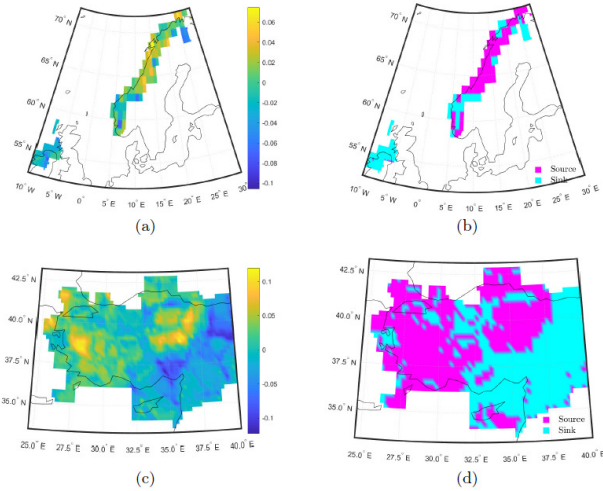
Figure 6. Two regional spatial networks from the SPI-6 Europe meteorological drought network. Degree centrality (a, c) and source-sink system (b, d).
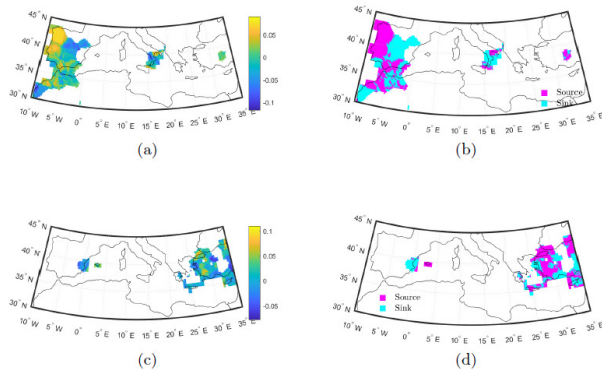
Figure 7. Two regional spatial networks from the SPI-9 Europe meteorological drought network. Degree centrality (a, c) and source-sink system (b, d).

(Figures 7c and 7d) we see the remaining part of Turkey with a small region of Spain. The only difference between the two communities, which may cause the distinction of this two regional clusters, is the fact that in the first case a portion of northern Africa and south Italy come into the picture as well. Looking at these two examples we highlight two main features: i) Portugal is still a big source (7a and 7b), as happened in the SPI-3 case, and ii) long connections strongly contribute in shaping the clusters' landscape, linking distant regions which are not generally related in the short accumulation periods' networks. This latter characteristic is even accentuated in the SPI-12 communities structures. We show in Figure 8 two examples taken from this last network. In the first one (Figures 8a and 8b) we see a community very similar to the one seen in Figure 7c: the majority of Turkey is still connected to the same nodes of eastern Spain, but, differently from before, this time the Spanish region is

a source for the rest of the community. This shows that the same nodes may play different roles in different accumulation
210   periods: in fact, they may belong to different communities or, as this latter examples show, they can still be part of similar
clusters but with a shift in the proportion of incoming links versus outgoing ones. In Figures 8c and 8d there is a clear vertical
separation in the source-sink system: the west part of both Great Britain and France is a source for the eastern regions of these
two territories. The cluster also includes a small region of the Scandinavian peninsula.
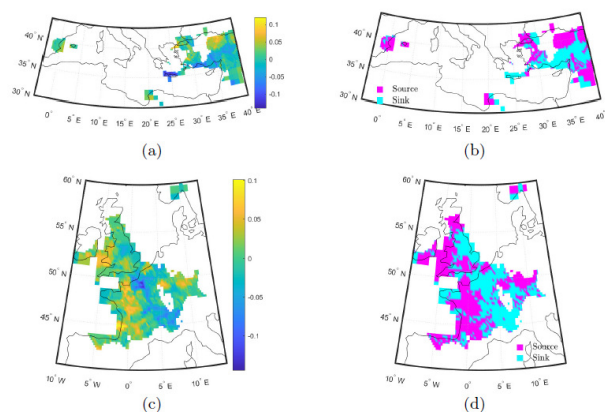
Figure 8. Two regional spatial networks from the SPI-12 Europe meteorological drought network. Degree centrality (a, c) and source-sink
system (b, d).

4   Conclusion

215   In this study we propose a method to build robust climate networks from data and to identify meteorological drought regions
and related source-sink systems in Europe.

Our networks are based on the synchronicity of drought's occurrences within a season and are constructed based on the
Standardized Precipitation Index for four accumulation periods, 3, 6, 9 and 12 months, highlighting similarities and differences
between those. The features of meteorological droughts for different timescales have never been investigated before through
220   the lens of network theory. Here, we find that long connections play a crucial role in shaping drought regions, and become
more and more important when long accumulations are considered. This suggest that, while short periods of precipitations'
deficiency (1 to 6 months) tend to evolve in confined regions, long lasting droughts (9 to 12 months) are likely to propagate
across large portions of the continent. Short meteorological drought events could be driven by regional climate systems, while
long ones by large scale patterns, like Rossby waves, but further studies are needed to better clarify the atmospheric precursors
225   of these long connections.

The Hamming procedure that we introduce here offers a new way to reduce the uncertainty of link attribution in unweighted
and undirected networks reconstruction from raw data, when there is no previous knowledge about the system under study.
This method could be potentially applied to different areas of study, and also be extended to weighted and directed graphs.

From these more reliable continental networks, we uncover regional communities by applying the Louvian algorithm, a well
230 recognized method for cluster identification. We believe that this way of partitioning a certain geographical area via network
theory concepts could be helpful in climate region identification, shaping them not via external classification or general climatic
variables, but based on the specific climate process under study.

Meteorological drought regions are separately studied identifying source-sink systems. These systems highlight the spatial
patterns along which the drought events have developed on average during the period 1980 - 2020. Moreover, they could be a
235 useful tool to use in forecasting these events in the sink nodes when the sources experience a drought condition.

Appendix A: Event Synchronization networks.

Starting from two event series i and j, an event l that occurs at i at time t_l^i is considered to be synchronized with an event m
that occurs at j at time t_m^j if $0 < t_l^i - t_m^j \leq \tau_{lm}^{ij}$, where

$$\tau_{lm}^{ij} = min\{t_{l+1}^i - t_l^i, t_l^i - t_{l-1}^i, t_{m+1}^j - t_m^j, t_m^j - t_{m-1}^j, 8\}/2. \tag{A1}$$

240 Notice that we set a maximum time lag of 4 months above which the possible synchronizations between two nodes are
disregarded. This means that the synchronicity between two locations is considered as such if it happens at most in the timescale
of a season.

A score J_{lm}^{ij} is assigned for every couple of events l and m in i and j according to the following rule:

$$J_{lm}^{ij} = \begin{cases} 1, & \text{if } 0 < t_l^i - t_m^j \leq \tau_{lm}^{ij}, \\ 1/2, & \text{if } t_l^i = t_m^j, \\ 0, & \text{else.} \end{cases} \tag{A2}$$

245 Finally, the number of times an event appears in i shortly after it occurs in j is counted

$$c(i|j) = \sum_{l=1}^{L} \sum_{m=1}^{M} J_{lm}^{ij}, \tag{A3}$$

where L and M are the total number of events in i and j respectively. The symmetrical Q_{ij} and the antisymmetrical q_{ij}
synchronization scores are then defined as follows

$$Q_{ij} = \frac{c(i|j) + c(j|i)}{\sqrt{ML}}, \qquad q_{ij} = \frac{c(i|j) - c(j|i)}{\sqrt{ML}}. \tag{A4}$$

250 The symmetrical score is suited for undirected networks while the antisymmetrical one contains the additional information
of the overall direction of the synchronicity between i and j: if there is a majority of events happening at i after they appear at j
compared to how many develop at j after taking place at i, then q_{ij} will be positive, with link's direction from j to i. Viceversa,
the sign will be negative, with direction of the link from i to j. The value of the antisymmetrical score represents the percentage
of times the j's events precede i's (or viceversa, depending on the sign), and serve as weight of the link. It can be interpreted as

255 the frequentist probability of observing an event happening at i (during the next four months) given that an event has happened at node j. It is possible to organize the synchronicity measures between each pair of nodes in an $N \times N$ matrix, where N is the number of nodes our spatial domain is discretized into. Each entry of the matrix lies between 0 and 1 and represent the strength of synchronization of node i and j. In principle, the synchronization between a node with itself is equal to 1, but we set it to 0 since self-loops are not meaningful in this context. We use q_{ij} for the weighted and directed community-specific networks,

260 while Q_{ij} is used for the four continental graphs. In this latter case, we even pass to an unweighted representation, recovering the adjacency matrix A_{ij} by preserving only the links with a synchronization score Q_{ij} greater than a certain threshold θ:

$$
A_{ij} = \begin{cases} 1, & \text{if } Q_{ij} \geq \theta \\ 0, & \text{else.} \end{cases} \tag{A5}
$$

The choice of the threshold is conducted via the Hamming distance procedure.

Appendix B: Hamming distance procedure.

265 We divide the complete 1981-2020 data-set into two sub-databases, one from 1981 to 2000 and another from 2001 to 2020. Then, we build one sub-network for each of the two time interval and for every possible cut-off threshold in terms of percentage of strongest preserved links (from 1 to 100). Notice that the two sub-databases are independent from each other, deriving from observations sampled in different periods of time.

Hence, we obtain two hundred different Europe's undirected and unweighted drought networks. Since our aim is to build

270 a single network as representative as possible of Europe's base meteorological drought conditions for the whole period 1981-2020, we assume the differences between the two sub-networks 1981-2000 and 2001-2020 to be minimum, since they are reproducing the same processes using independent data. In other words, if two locations i and j are drought-synchronized, this should results in both sub-networks. The underlying assumption we make here is that even if the frequency and duration of meteorological drought events may be changing due to climate change, the physical mechanism that shapes the locations'

275 synchronization in drought events occurrences does not change in time and the resulting spatial structure modeled with the climate network remains reasonably stable.

For every cut-off threshold we count the differences between the two sub-networks via the Hamming distance, which measures the global probability of non-equal entries in the two adjacency matrices:

$$
H(A^{1981-2000}, A^{2001-2020}) = \frac{1}{N^2} \sum_{i,j} XOR(A_{ij}^{1981-2000}, A_{ij}^{2001-2020}), \tag{B1}
$$

280 where

$$
XOR(A_{ij}^{1981-2000}, A_{ij}^{2001-2020}) = \begin{cases} 1 & \text{if } A_{ij}^{1981-2000} \neq A_{ij}^{2001-2020} \\ 0 & \text{else.} \end{cases} \tag{B2}
$$

The procedure is depicted in Figure B1.

Even if we expect the two sub-networks to be similar for each cut-off threshold, they can never be identical due to noise and climate's internal variability. Therefore, we select as definitive cut-off threshold θ_{def} the one for which the Hamming distance
285   is below 5%:

$$\theta_{def} : H(\theta_1) < H(\theta_2) < ... < H(\theta_{def}) \leq 0.05 < H(\theta_{def+1}). \tag{B3}$$

This requirement is satisfied for each of the four continental networks if we preserve the top 4% of links (Figure B2). Consequently, an unweighted and undirected link is placed every time the value of synchronization between two nodes is above the 96-th percentile. We want this threshold to be the same for the four cases in order to compare the resulting networks,
290   which are this way characterized by approximately the same link density.

The definitive continental networks are therefore so constructed for each of the four accumulation periods: (a) two undirected and unweighted sub-networks are retrieved from the data 1981-2000 and 2001-2020 respectively, taking the 96-th percentile as cut-off threshold and (b) the two sub-networks are intersected, taking only the common links between the two to form the final 1981-2020 Europe meteorological drought network.
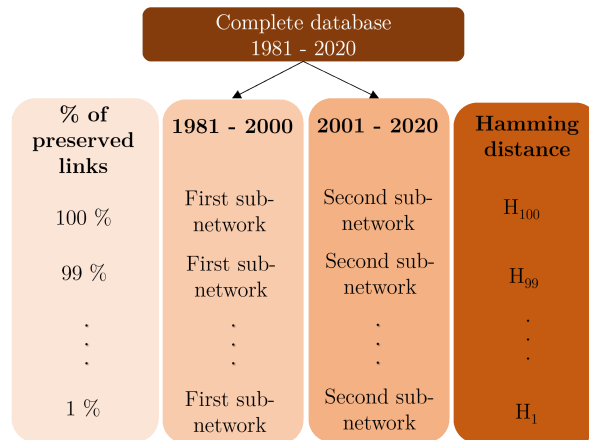
Figure B1. Procedure to select the percentage of strongest links to preserve. The original database is split symmetrically into two sub-databases. For each of them and for every cut-off threshold an undirected and unweighted Event Synchronization network is constructed. Every pair of sub-networks is used to compute the Hamming Distance.
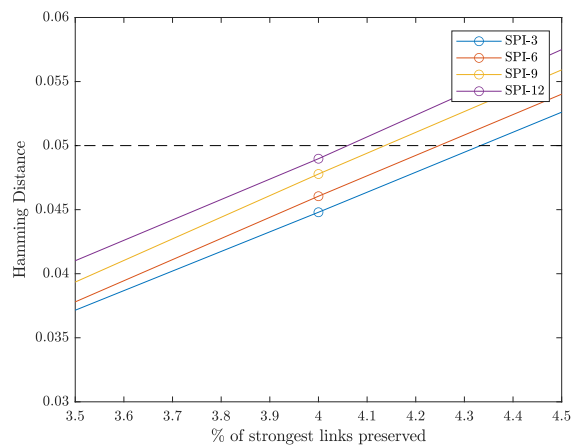
Figure B2. The Hamming Distance as a function of the percentage of strongest link preserved. By choosing the 96-th percentile as cut-off threshold (preserving the top 4% of links) the differences between the two sub-networks are below 5% in each of the four cases.

295 *Author contributions.* All authors contributed to planning the work and writing and editing the manuscript.

Competing interests. The authors declare that they have no conflict of interest.

References

Bastos, A., Fu, Z., Ciais, P., Friedlingstein, P., Sitch, S., Pongratz, J., Weber, U., Reichstein, M., Anthoni, P., Arneth, A., et al.: Impacts of extreme summers on European ecosystems: a comparative analysis of 2003, 2010 and 2018, Philosophical Transactions of the Royal Society B, 375, 20190 507, 2020.

Beillouin, D., Schauberger, B., Bastos, A., Ciais, P., and Makowski, D.: Impact of extreme weather conditions on European crop production in 2018, Philosophical Transactions of the Royal Society B, 375, 20190 510, 2020.

Bevacqua, A. G., Chaffe, P. L., Chagas, V. B., and AghaKouchak, A.: Spatial and temporal patterns of propagation from meteorological to hydrological droughts in Brazil, Journal of Hydrology, 603, 126 902, 2021.

Blondel, V. D., Guillaume, J.-L., Lambiotte, R., and Lefebvre, E.: Fast unfolding of communities in large networks, Journal of statistical mechanics: theory and experiment, 2008, P10 008, 2008.

Boccaletti, S., Latora, V., Moreno, Y., Chavez, M., and Hwang, D.-U.: Complex networks: Structure and dynamics, Physics reports, 424, 175–308, 2006.

Boers, N., Bookhagen, B., Marwan, N., Kurths, J., and Marengo, J.: Complex networks identify spatial patterns of extreme rainfall events of the South American Monsoon System, Geophysical Research Letters, 40, 4386–4392, 2013.

Boers, N., Goswami, B., Rheinwalt, A., Bookhagen, B., Hoskins, B., and Kurths, J.: Complex networks reveal global pattern of extreme-rainfall teleconnections, Nature, 566, 373–377, 2019.

Böhnisch, A., Mittermeier, M., Leduc, M., and Ludwig, R.: Hot Spots and Climate Trends of Meteorological Droughts in Europe–Assessing the Percent of Normal Index in a Single-Model Initial-Condition Large Ensemble, Frontiers in Water, 3, 716 621, 2021.

Ciemer, C., Rehm, L., Kurths, J., Donner, R. V., Winkelmann, R., and Boers, N.: An early-warning indicator for Amazon droughts exclusively based on tropical Atlantic sea surface temperatures, Environmental Research Letters, 15, 094 087, 2020.

Cook, B. I., Mankin, J. S., Marvel, K., Williams, A. P., Smerdon, J. E., and Anchukaitis, K. J.: Twenty-first century drought projections in the CMIP6 forcing scenarios, Earth's Future, 8, e2019EF001 461, 2020.

Donges, J. F., Zou, Y., Marwan, N., and Kurths, J.: The backbone of the climate network, EPL (Europhysics Letters), 87, 48 007, 2009.

Doughty, C. E., Metcalfe, D., Girardin, C., Amézquita, F. F., Cabrera, D. G., Huasco, W. H., Silva-Espejo, J., Araujo-Murakami, A., Da Costa, M., Rocha, W., et al.: Drought impact on forest carbon dynamics and fluxes in Amazonia, Nature, 519, 78–82, 2015.

EDO: Standardized Precipitation Index (SPI), Tech. rep., European Drought Observatory, 2020.

Edwards, D. C.: Characteristics of 20th Century drought in the United States at multiple time scales., Tech. rep., Air Force Inst of Tech Wright-Patterson Afb Oh, 1997.

Fan, J., Meng, J., Ludescher, J., Chen, X., Ashkenazy, Y., Kurths, J., Havlin, S., and Schellnhuber, H. J.: Statistical physics approaches to the complex Earth system, Physics reports, 896, 1–84, 2021.

Feng, X., Merow, C., Liu, Z., Park, D. S., Roehrdanz, P. R., Maitner, B., Newman, E. A., Boyle, B. L., Lien, A., Burger, J. R., et al.: How deregulation, drought and increasing fire impact Amazonian biodiversity, Nature, 597, 516–521, 2021.

Gupta, S., Boers, N., Pappenberger, F., and Kurths, J.: Complex network approach for detecting tropical cyclones, Climate Dynamics, 57, 3355–3364, 2021.

Guttman, N. B.: Accepting the standardized precipitation index: a calculation algorithm 1, JAWRA Journal of the American Water Resources Association, 35, 311–322, 1999.

Iturbide, M., Gutiérrez, J. M., Alves, L. M., Bedia, J., Cerezo-Mota, R., Cimadevilla, E., Cofiño, A. S., Di Luca, A., Faria, S. H., Gorodet-skaya, I. V., et al.: An update of IPCC climate reference regions for subcontinental analysis of climate model data: definition and aggregated

335   datasets, Earth System Science Data, 12, 2959–2970, 2020.

Jian, L. and Hao-Ming, C.: Atlas in the IPCC AR6, Advances in Climate Change Research, 17, 726, 2021.

Konapala, G., Mondal, S., and Mishra, A.: Quantifying spatial drought propagation potential in North America using complex network theory, Water Resources Research, 58, e2021WR030 914, 2022.

Kurths, J., Agarwal, A., Shukla, R., Marwan, N., Rathinasamy, M., Caesar, L., Krishnan, R., and Merz, B.: Unravelling the spatial diversity

340   of Indian precipitation teleconnections via a non-linear multi-scale approach, Nonlinear Processes in Geophysics, 26, 251–266, 2019.

Lloyd-Hughes, B.: The impracticality of a universal drought definition, Theoretical and Applied Climatology, 117, 607–611, 2014.

Ludescher, J., Martin, M., Boers, N., Bunde, A., Ciemer, C., Fan, J., Havlin, S., Kretschmer, M., Kurths, J., Runge, J., et al.: Network-based forecasting of climate phenomena, Proceedings of the National Academy of Sciences, 118, e1922872 118, 2021.

Malik, N., Bookhagen, B., Marwan, N., and Kurths, J.: Analysis of spatial and temporal extreme monsoonal rainfall over South Asia using

345   complex networks, Climate dynamics, 39, 971–987, 2012.

Marinho Ferreira Barbosa, P., Masante, D., Arias-Muñoz, C., Cammalleri, C., De Jager, A., Magni, D., Mazzeschi, M., Mccormick, N., Naumann, G., Spinoni, J., and Vogt, J.: Droughts in Europe and Worldwide 2019-2020, JRC125320, 2021.

McKee, T. B., Doesken, N. J., Kleist, J., et al.: The relationship of drought frequency and duration to time scales, in: Proceedings of the 8th Conference on Applied Climatology, vol. 17, pp. 179–183, Boston, MA, USA, 1993.

350   Mishra, A. K. and Singh, V. P.: A review of drought concepts, Journal of hydrology, 391, 202–216, 2010.

Mukherjee, S., Mishra, A., and Trenberth, K. E.: Climate change and drought: a perspective on drought indices, Current Climate Change Reports, 4, 145–163, 2018.

Naumann, G., Cammalleri, C., Mentaschi, L., and Feyen, L.: Increased economic drought impacts in Europe with anthropogenic warming, Nature Climate Change, 11, 485–491, 2021.

355   Newman, M. E.: Modularity and community structure in networks, Proceedings of the national academy of sciences, 103, 8577–8582, 2006.

Quiroga, R. Q., Kreuz, T., and Grassberger, P.: Event synchronization: a simple and fast method to measure synchronicity and time delay patterns, Physical review E, 66, 041 904, 2002.

Seneviratne, S., Nicholls, N., Easterling, D., Goodess, C., Kanae, S., Kossin, J., Luo, Y., Marengo, J., McInnes, K., Rahimi, M., et al.: Changes in climate extremes and their impacts on the natural physical environment, 2012.

360   Spinoni, J., Naumann, G., Vogt, J. V., and Barbosa, P.: The biggest drought events in Europe from 1950 to 2012, Journal of Hydrology: Regional Studies, 3, 509–524, 2015.

Spinoni, J., Naumann, G., Vogt, J., and Barbosa, P.: Meteorological droughts in europe: events and impacts-past trends and future projections, 2016.

Spinoni, J., Naumann, G., and Vogt, J. V.: Pan-European seasonal trends and recent changes of drought frequency and severity, Global and

365   Planetary Change, 148, 113–130, 2017.

Spinoni, J., Vogt, J. V., Naumann, G., Barbosa, P., and Dosio, A.: Will drought events become more frequent and severe in Europe?, International Journal of Climatology, 38, 1718–1736, 2018.

Spinoni, J., Barbosa, P., Bucchignani, E., Cassano, J., Cavazos, T., Cescatti, A., Christensen, J. H., Christensen, O. B., Coppola, E., Evans, J. P., et al.: Global exposure of population and land-use to meteorological droughts under different warming levels and SSPs: a CORDEX-

370   based study, International Journal of Climatology, 41, 6825–6853, 2021.

Spinoni J, Naumann G, V. J. and P, B.: Meteorological Droughts in Europe: Events and Impacts: Past Trends and Future Projections, JRC100394, 2016.

Stolbova, V., Martin, P., Bookhagen, B., Marwan, N., and Kurths, J.: Topology and seasonal evolution of the network of extreme precipitation over the Indian subcontinent and Sri Lanka, Nonlinear Processes in Geophysics, 21, 901–917, 2014.

375 Taufik, M., Torfs, P. J., Uijlenhoet, R., Jones, P. D., Murdiyarso, D., and Van Lanen, H. A.: Amplification of wildfire area burnt by hydrological drought in the humid tropics, Nature Climate Change, 7, 428–431, 2017.

Tsonis, A. A., Swanson, K. L., and Roebber, P. J.: What do networks have to do with climate?, Bulletin of the American Meteorological Society, 87, 585–596, 2006.

Tsonis, A. A., Swanson, K. L., and Wang, G.: On the role of atmospheric teleconnections in climate, Journal of Climate, 21, 2990–3001,
380 2008.

Vicente-Serrano, S. M., Domínguez-Castro, F., Murphy, C., Hannaford, J., Reig, F., Peña-Angulo, D., Tramblay, Y., Trigo, R. M., Mac Donald, N., Luna, M. Y., et al.: Long-term variability and trends in meteorological droughts in Western Europe (1851–2018), International journal of climatology, 41, E690–E717, 2021.

Walthall, C. L., Hatfield, J., Backlund, P., Lengnick, L., Marshall, E., Walsh, M., Adkins, S., Aillery, M., Ainsworth, E., Ammann, C.,
385 et al.: Climate change and agriculture in the United States: Effects and adaptation, United States Department of Agriculture, Agricultural Research Services . . . , 2013.

Wehner, M., Seneviratne, S., Zhang, X., Adnan, M., Badi, W., Dereczynski, C., Di Luca, A., Ghosh, S., Iskandar, I., Kossin, J., et al.: Weather and climate extreme events in a changing climate, in: AGU Fall Meeting Abstracts, vol. 2021, pp. U13B–11, 2021.

Wei, W., Zhang, J., Zhou, L., Xie, B., Zhou, J., and Li, C.: Comparative evaluation of drought indices for monitoring drought based on remote
390 sensing data, Environmental Science and Pollution Research, 28, 20 408–20 425, 2021.

Wilhite, D. A. and Glantz, M. H.: Understanding: the drought phenomenon: the role of definitions, Water international, 10, 111–120, 1985.

WMO: Atlas of Mortality and Economic Losses from Weather, Climate and Water Extremes (1970–2019), 1267, 2021.

Zanin, M., Sousa, P., Papo, D., Bajo, R., García-Prieto, J., Pozo, F. d., Menasalvas, E., and Boccaletti, S.: Optimizing functional network representation of multivariate time series, Scientific reports, 2, 1–6, 2012.

395 Zargar, A., Sadiq, R., Naser, B., and Khan, F. I.: A review of drought indices, Environmental Reviews, 19, 333–349, 2011.

Zhao, T. and Dai, A.: Uncertainties in historical changes and future projections of drought. Part II: model-simulated historical and future drought changes, Climatic Change, 144, 535–548, 2017.